Terahertz reflection spectroscopy of Debye relaxation in polar liquids [Invited]

Uffe Møller,[1] David G. Cooke,[1] Koichiro Tanaka,[2,3] and Peter Uhd Jepsen[1,*]

[1]*DTU Fotonik—Department of Photonics Engineering, Technical University of Denmark, Ørsteds Plads, Bldg. 343, DK-2800 Kgs. Lyngby, Denmark*
[2]*Department of Physics, Graduate School of Science, Kyoto University, Kitashirakawa, Sakyo-ku, Kyoto 606-8502, Japan*
[3]*Institute for Integrated Cell-Material Sciences, Kyoto University, Yoshidakonoe-cho, Sakyo-ku, Kyoto 606-8501, Japan*
[*]*Corresponding author: puje@fotonik.dtu.dk*

Received August 13, 2009; accepted August 13, 2009;
posted August 17, 2009 (Doc. ID 115700); published August 28, 2009

Terahertz (THz) radiation interacts strongly with the intermolecular hydrogen-bond network in aqueous liquids. The dielectric properties of liquid water and aqueous solutions in the THz spectral region are closely linked to the microscopic dynamics of the liquid solution, and hence THz spectroscopy offers an important insight into fundamental intermolecular interactions in polar liquids. At the same time, the strong and characteristic interaction between THz radiation and liquids offers a methodology for the classification of liquids inside containers, and hence the THz region is suitable for remote detection of some of the properties of bottled liquids. Here we present a review of THz spectroscopy and modeling of water–ethanol mixtures, and establish a link between the dielectric function of water–ethanol mixtures and some of their thermodynamic properties. We then review how the knowledge of the dielectric function of aqueous mixtures can be used for inspection of liquids inside bottles. Finally we draw up some of the limits to the applicability of THz reflection spectroscopy in the identification of dangerous liquids.

OCIS codes: 300.6495, 120.4530, 010.4290, 120.4290.

1. INTRODUCTION

With the possible exception of ethanol, water is the most important liquid for mankind. Hence it is not surprising that the properties of water have been investigated since the beginning of science. In spite of the apparently simple geometry of the water molecule, liquid water has a range of surprising physical and thermodynamic properties, which include strong deviations from ideal mixing behavior, higher density than solid water (ice I), and exothermic mixing properties with certain other liquids that can form hydrogen bonds. All these properties stem, in one way or another, from the unique property of the water molecule to form a tetrahedral arrangement of hydrogen bonds to its neighboring molecules, thereby forming a highly dynamic network of virtually infinite extent of interconnected molecules.

The optical properties of bulk water have been investigated at all wavelengths normally associated with electromagnetic radiation. In Fig. 1 we show the absorption coefficient (on a logarithmic scale) and the index of refraction (on a linear scale) as function of frequency (lower, horizontal axis) or wavenumber (upper, horizontal axis) [1].

The gray area indicates the part of the THz spectrum typically accessed by THz time-domain spectroscopy (THz-TDS) techniques, and the visible region of the spectrum is indicated by the narrow bar. The figure shows that THz-TDS has access to the part of the dielectric response of water that lies below the vibrational bands in the infrared.

The large dipole moment of the water molecule in interplay with the dynamic intermolecular network of hydrogen bonds forms a highly complex many-body system. This system interacts collectively in a strong and characteristic manner with electro-magnetic radiation at microwave and THz frequencies. This is due to the fact that the typical time scales involved in relaxation dynamics of water molecules displaced or rotated from their equilibrium positions falls in the picosecond to subpicosecond range. Thus far-infrared or THz spectroscopy is a versatile tool for the study of the collective properties of water, in particular, and of hydrogen-bonded liquids in general.

When a molecule is solvated or dispersed in water, the water molecules will naturally rearrange themselves in order to accommodate the molecule. This rearrangement will influence the local structure of the dynamic intermolecular hydrogen bond network, and thus the THz dielectric properties will also change locally. This effect has been demonstrated in spectroscopic studies of sucrose in water, where an analysis based on the broadband dielectric properties of the solution in the THz range made it possible to measure the size of the solvation shell around the sucrose molecules [2]. Other experiments, using narrow-band THz radiation rather than a broadband spectroscopic source, have revealed the size of the solvation shell around proteins and carbohydrates solvated in water [3,4]. Related work on water contained in inverse micelles [5–7] demonstrated that nanometer-sized pools of water behave distinctively different from bulk water, due to mechanical resonances of the spherical water in-

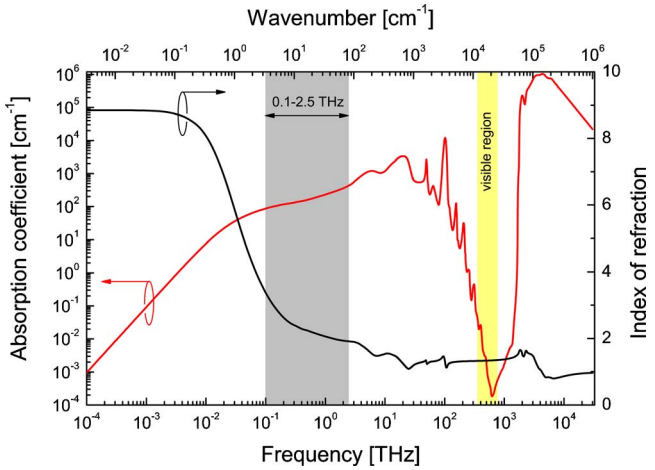

Fig. 1. (Color online) Absorption spectrum (red curve, logarithmic scale) and index of refraction (black curve, linear scale) as function of frequency (lower horizontal scale) and wavenumber (upper, horizontal scale). The gray area indicates the 0.1–2.5 THz region, and the narrow yellow shaded area indicates the visible part of the spectrum.

clusion. It was demonstrated that extended interfaces of liquid water with a thickness of a few nanometers, condensed on the surface of a parallel-plate waveguide, behaves like bulk water [8], whereas strong deviations from bulk behavior was observed in the dielectric spectrum of submonolayer films of water absorbed on the surface of hydrophilic aerogels [9]. All these reports clearly demonstrate that the three-dimensional environment of water molecules in the liquid state plays a defining role for the local dielectric response of the liquid at distances on the nanometer scale from solvated molecules or from interfaces. These works have also demonstrated that at distances greater than, for instance, the radius of the solvation shell surrounding a molecule in liquid water, the dielectric properties of the water solvent are identical, or at least in practice indistinguishable from the properties of bulk water. Importantly, this dielectric response can be sensed by spectroscopy in the THz frequency range.

The paper is organized as follows: In Section 2 we describe different methods based on reflection spectroscopy for the measurement of the full dielectric function of strongly absorbing liquids in the THz range. In Section 3 we then briefly discuss the derivation of the Debye model of dielectric relaxation. In Section 4 we then describe a detailed investigation of the dielectric function of water–ethanol mixtures. In the more applications-oriented Section 5 we describe how the dielectric properties of liquids can be inspected though the wall material of bottles, and in Section 6 we show selected examples of the application of reflection-type THz spectroscopy for characterization of liquids that may be classified as dangerous. These liquids include hydrogen peroxide, a strong oxidizing agent, as well as the liquid fuel components nitromethane and nitroethane.

2. EXPERIMENTAL METHODS FOR REFLECTION THz SPECTROSCOPY

With the invention of far-infrared Fourier transform infrared spectroscopy (FTIR) and later THz-TDS, spectroscopic investigations of liquid water in the far infrared has been a recurring topic for the past 30 years.

Spectroscopy of liquids is typically carried out in either a transmission geometry or in a reflection geometry, depending on the absorption strength of the liquid. The highest absorption coefficient that can be measured in a transmission experiment is limited by the dynamic range of the spectrometer, here defined as the frequency-dependent reference signal amplitude with respect to the noise floor of the experiment [10]. In contrast it is the signal-to-noise ratio of the spectrometer, i.e., frequency-dependent fluctuations of the signal strength, that determines the largest measurable absorption coefficient in a reflection experiment, since the absorption of the sample is detected as a small additional phase of the reflected signal [10].

Due to the rather strong absorption of polar liquids, and in particular of water, spectroscopy in the THz region of such liquids is typically carried out in a reflection geometry on bulk quantities of the liquid or by transmission through a very thin liquid layer. While THz transmission measurements of liquid water are certainly possible for thin water layers, the subsequent analysis becomes plagued with multiple reflections of the THz beam in the water cell, especially at low frequencies. In the region above 1 THz, transmission experiments are difficult due to strong absorption, and in recent work targeting the frequency range of 1–6 THz, reflection-type spectroscopy seems to be the method of choice. Here we will thus briefly review different techniques applied for reflection THz spectroscopy.

Historically, the technique of dispersive Fourier transform spectroscopy (DFTS) [11] was the first method for accurate determination of the full dielectric function of materials in the far infrared. Afsar and Hasted used DFTS [12] to characterize the full dielectric function of liquid water in the 0.2–13.5 THz range (6–450 cm^{-1}). In their spectroscopic setup, water was kept behind a single-crystal, high-resistivity silicon window, transparent to the far-infrared radiation but with sufficiently high and constant index of refraction [13] to also serve as a useful beam splitter for the THz radiation. The liquid cell was placed in one of the arms of the modified Michelson interferometer in the spectrometer, as illustrated schematically in Fig. 2(a). Hence phase-sensitive measurements were possible by measuring the interferogram $I(\tau)$ of the incoherent, broadband light source. This allowed a direct evaluation of both the real and the imaginary part of the frequency-dependent permittivity $\hat{\epsilon}(\nu)=\epsilon'(\nu)+i\epsilon''(\nu)$ from the experimental data.

In DFTS, temporally separated interferograms of the incoherent light reflected from the different dielectric interfaces in the sample arm of the spectrometer are recorded by scanning the position $\tau=2x/c$ of the mirror in the variable arm of the interferometer. The part of the interferogram $I_{wa}(\tau)$ associated with the window–air interface of the empty cell is used as a reference for the sample interferogram $I_{wl}(\tau)$ from the window–liquid interface of the filled liquid cell. The ratio of the Fourier transformations of these interferograms can then, in combination with the standard expressions for the Fresnel reflection

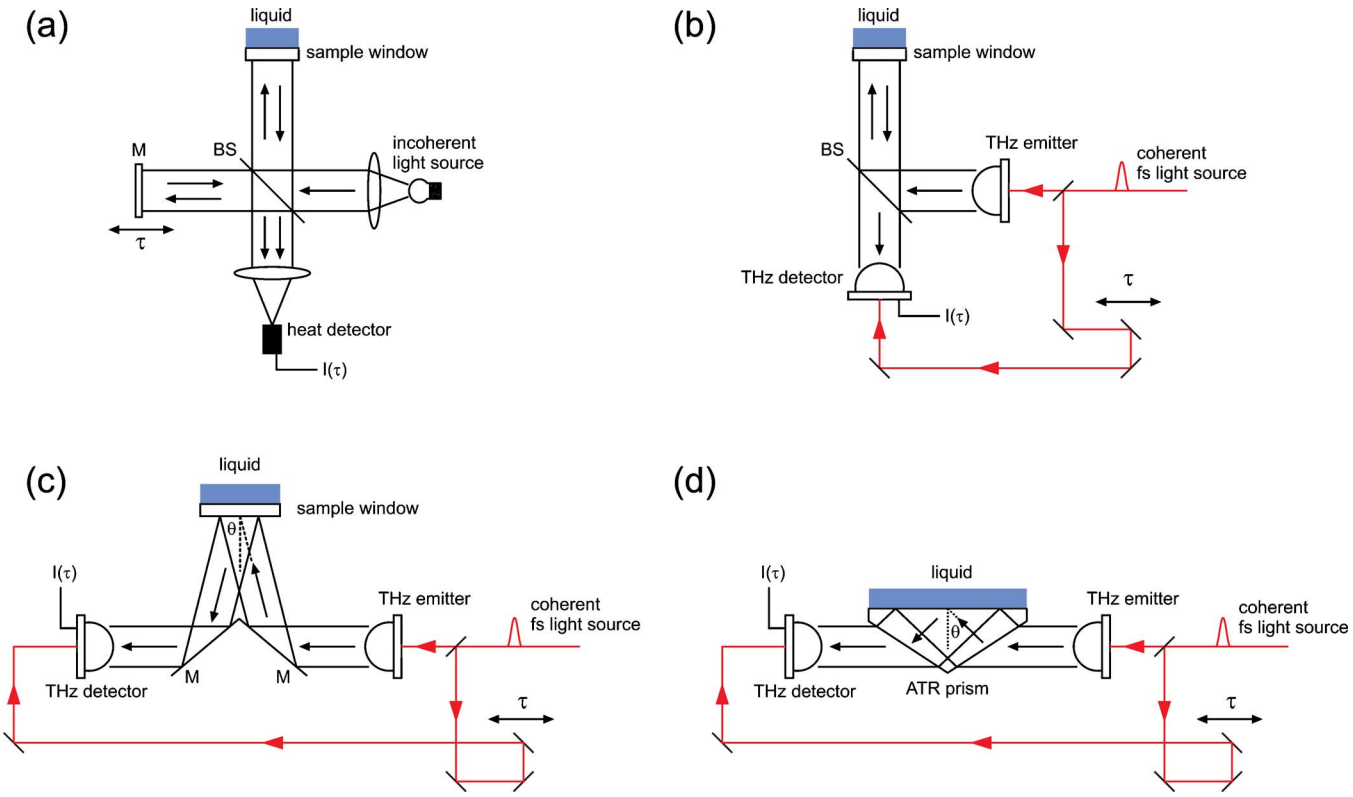

Fig. 2. (Color online) Experimental configurations for (a) dispersive Fourier transform spectroscopy (DFTS), (b) normal-incidence reflection THz time-domain spectroscopy (THz-TDS), (c) generalized reflection THz-TDS with an incidence angle θ, and (d) attenuated total reflection (ATR) THz-TDS with an internal angle θ larger than the total internal reflection angle.

coefficients at the interfaces, be used for the calculation of the optical properties of the liquid:

$$R\exp(i\phi)=\frac{\mathcal{F}\{I_{wl}(\tau)\}}{\mathcal{F}\{I_{wa}(\tau)\}}=\frac{\hat{I}_{wl}(\nu)}{\hat{I}_{wa}(\nu)}=\frac{\hat{r}_{wl}(\nu)}{r_{wa}(\nu)}$$

$$=\frac{(\hat{n}_l(\nu)-n_w(\nu))(1+n_w(\nu))}{(\hat{n}_l(\nu)+n_w(\nu))(1-n_w(\nu))}, \quad (1)$$

where R and ϕ are the measured amplitude and phase of the ratio of the two interferograms and $\mathcal{F}$ denotes the Fourier transformation. When inverted, Eq. (1) gives the complex index of refraction of the liquid, $\hat{n}_l(\nu)=n_l(\nu)+i\alpha_l(\nu)c/(4\pi\nu)$, assuming that the index of refraction n_w of the window material is known:

$$n_l=\frac{1-R^2\left(\frac{1-n_w}{1+n_w}\right)^2}{1+R^2\left(\frac{1-n_w}{1+n_w}\right)^2-2R\cos\phi\left(\frac{1-n_w}{1+n_w}\right)}, \quad (2)$$

$$\alpha_l=\frac{4\pi\nu}{c}\frac{2R\sin\phi\left(\frac{1-n_w}{1+n_w}\right)}{1+R^2\left(\frac{1-n_w}{1+n_w}\right)^2-2R\cos\phi\left(\frac{1-n_w}{1+n_w}\right)}. \quad (3)$$

THz-TDS [14] is a modern spectroscopic technique with much of the same functionality as DFTS, and with several fundamental as well as practical advantages compared to FTIR spectroscopy. In THz-TDS a short burst of coherent light in the THz region is generated and detected either by the ultrafast photoconductive response in miniature photoconductive switches excited by femtosecond laser pulses [15] or by optical rectification of ultrafast laser pulses and free-space electro-optic sampling in a nonlinear crystal [16]. In both techniques, a femtosecond laser pulse train is split into two portions by a beamsplitter, where one portion is used for generation of the THz pulse, consisting typically of a single cycle of the electromagnetic field, and the second, delayed portion is used for time-resolved sampling of the electrical field of the THz signal.

Thrane *et al.* [17] established a reflection-type THz-TDS technique with an experimental arrangement of the liquid cell similar to that in [12], adapted to the technique of reflection THz-TDS, with normal incidence of the THz field onto the liquid surface. This experimental geometry is illustrated in Fig. 2(b). In the geometry shown here, the full set of spectroscopic data is obtained within the same temporal scan, by using the reflection from the interface between air and window material as the reference signal $E_r(\tau)$ and the reflection from the interface between the window and the liquid as the sample signal $E_s(\tau)$. The sample signal is separated in time from the reference signal due to the propagation delay of the sample signal

through the window material of thickness d_w. With normal incidence of the THz beam on the window, the ratio of the spectra of the sample and reference pulses is

$$\frac{\mathcal{F}\{E_s(\tau)\}}{\mathcal{F}\{E_r(\tau)\}} = \frac{\hat{E}_s(\nu)}{\hat{E}_r(\nu)} = \frac{t_{aw}t_{wa}}{r_{aw}} \exp\left(i\frac{4\pi n_w d_w \nu}{c}\right)\frac{\hat{n}_l - n_w}{\hat{n}_l + n_w} \Leftrightarrow R\exp(i\phi)$$

$$= \frac{\hat{E}_s(\nu)}{\hat{E}_r(\nu)}\frac{r_{aw}}{t_{aw}t_{wa}} \exp\left(-i\frac{4\pi n_w d_w \nu}{c}\right) = \frac{\hat{n}_l - n_w}{\hat{n}_l + n_w}, \quad (4)$$

where R and ϕ are the measured spectral amplitude and phase of the ratio of the sample- and reference signals, corrected for the transmission and reflection coefficients of the air–window interface and the acquired phase due to propagation through the window material.

Inverting Eq. (4) yields the index of refraction and absorption coefficient of the liquid:

$$n_l = \frac{n_w(1-R^2)}{1+R^2+2R\cos\phi}, \quad (5)$$

$$\alpha_l = \frac{4\pi n_w \nu}{c}\frac{-2R\sin\phi}{1+R^2+2R\cos\phi}. \quad (6)$$

The methodology described here for the calculation of the dielectric properties of the liquid can be extended to an analysis at non-normal incidence at an angle θ of the THz beam on the sample window. This experimental geometry is shown schematically in Fig. 2(c). Compared to normal-incidence reflection spectroscopy, the configuration with non-normal incidence of the THz beam has a significantly higher signal strength, since the THz beam splitter is no longer required. In this geometry the generalized reflection and transmission coefficients must be used, and also the polarization state of the THz beam becomes important [18]. Due to the many possible configurations, we refrain from presenting the full expressions for the determination of the optical constants of the liquid, but we refer to the discussion in [18].

The most sensitive method for determination of the full dielectric function of a strongly absorbing liquid is offered by attenuated total reflection (ATR) THz-TDS [19,20]. In this configuration the THz beam is transmitted through a Dove prism where it undergoes total internal reflection at a facet of the prism in contact with the liquid. The geometry of an ATR THz-TDS system is schematically shown in Fig. 2(d). The angle θ refers to the internal incidence angle of the THz beam onto the interface towards the liquid. The highest sensitivity to small changes in the dielectric properties of the sample is obtained when that incidence angle is larger than, but close to, the critical angle for total internal reflection. The measurement is carried out by recording a reference pulse $E_r(\tau)$ transmitted through the prism with air above the interface and subsequently a sample pulse $E_s(\tau)$ recorded with liquid in contact with the prism. The ratio of the spectra of these two signals is, as in the previous cases discussed here, analyzed in order to extract the complex index of refraction of the liquid. If we assume p-polarization of the THz light incident on the ATR interface we have [19]

$$R\exp(i\phi) = \frac{\mathcal{F}\{E_s(\tau)\}}{\mathcal{F}\{E_r(\tau)\}} = \frac{\hat{E}_s(\nu)}{\hat{E}_r(\nu)} = \frac{\hat{r}^p_{wl}}{\hat{r}^p_{wa}} \Leftrightarrow \hat{r}^p_{wl} = \hat{r}^p_{wa}R\exp(i\phi), \quad (7)$$

where R and ϕ again represent the amplitude and phase of the ratio of the spectra of the sample- and reference pulses.

Using the Fresnel reflection coefficients for total internal reflection of p-polarized light, Eq. (7) can be inverted to find an expression for the complex permittivity $\hat{\epsilon}_l = \epsilon_l' + i\epsilon_l'' \equiv \hat{n}_l^2$ [19]:

$$\hat{\epsilon}_l = \frac{B \pm \sqrt{B^2 - AB\sin^2 2\theta}}{2A\cos^2\theta}, \quad (8)$$

where $A=(\hat{r}^p_{wl}-1)^2$ and $B=(\hat{r}^p_{wl}+1)^2$. All typical material systems show a positive ϵ'' and hence the solution with $\epsilon_l'' > 0$ should be chosen.

3. DEBYE MODEL OF THE DIELECTRIC FUNCTION OF POLAR LIQUIDS

The most widely accepted phenomenological description of the complex frequency-dependent dielectric function $\hat{\epsilon}(\omega)$ of polar, nonconductive ($\sigma_{DC}=0$) liquids is based on the Debye model and extensions of the Debye model. Here we will briefly summarize a derivation of the Debye model of dielectric relaxation [21].

When a dielectric material is subject to a sudden electric field E then the induced total polarization P will have two contributions: the near-instantaneous electronic response P_1 and the slower dipolar response P_2. It is assumed that the rate of change of P_2 is proportional to the distance to the steady-state total polarization,

$$\frac{dP_2}{dt} = \frac{P - P_1 - P_2}{\tau}, \quad (9)$$

where τ is the characteristic relaxation time of the process. If an electric field is suddenly switched on at $t=0$ then the solution is

$$P_2(t) = (P - P_1)(1 - \exp(-t/\tau)), \quad (10)$$

showing the characteristic exponential behavior of the relaxation process in the Debye picture.

If a harmonic electric field at frequency ν, $E(t) = E_0\exp(-i2\pi\nu t)$, is applied to the material then the solution to Eq. (9) is

$$\frac{dP_2}{dt} = \frac{\epsilon_0(\epsilon_s - \epsilon_\infty)}{\tau}E_0\exp(i2\pi\nu t) - \frac{P_2}{t} \quad (11)$$

$$\Rightarrow P_2(t) = \frac{\epsilon_0(\epsilon_s - \epsilon_\infty)}{1 - i2\pi\nu\tau}E(t), \quad (12)$$

where it has been assumed that the total steady-state polarization is expressed as $P=\epsilon_0(\epsilon_s-1)E, \nu\to 0$ and the electronic polarization is $P_1=\epsilon_0(\epsilon_\infty-1)E$.

Using the known relation between the induced polarization and the applied field, $P=\epsilon_0(\epsilon-1)E$ we find the complex permittivity

$$\hat{\epsilon}(\nu)=\epsilon'(\nu)+i\epsilon''(\nu)=\epsilon_\infty+\frac{\epsilon_s-\epsilon_\infty}{1-i2\pi\nu\tau}. \tag{13}$$

From this derivation of the basic Debye permittivity spectrum it can be seen that, if several relaxation processes with different relaxation times take place in parallel, then the total dielectric function will be a simple sum of the individual contributions from each process.

Furthermore, in the general case the dielectric function of a polar liquid is determined by dielectric relaxation processes at the lowest frequencies and by vibrational modes (intermolecular and intramolecular) at higher frequencies. If we assume that N relaxation processes occur simultaneous with M homogeneously broadened vibrational modes then the general dielectric function can be expressed as

$$\hat{\epsilon}(\omega)=\sum_{j=1}^{N}\frac{\Delta\epsilon_j}{1-i\omega\tau_j}+\sum_{j=1}^{M}\frac{A_j}{\omega_j^2-\omega^2-i\omega\gamma_j}+\epsilon_\infty, \tag{14}$$

where the coefficients A_j are the vibrational amplitudes, $\omega_j/2\pi$ are the resonance frequencies, and γ_j are the damping rates of the jth vibrational mode.

As will be discussed in Section 4, up to three relaxation processes are required in the model in order to describe the dielectric response of ethanol and ethanol–water mixtures. The microscopic basis of the introduction of three relaxation processes is still debated in the literature, and it is important to note that it is not our goal to shed light on the fundamental question of the validity of the Debye model.

The Debye model with the incorporation of several relaxation processes is based on the assumption that these relaxation processes are independent of each other and take place in a parallel fashion [22]. This assumption is not obvious, and a deeper insight into the fundamental nature of the relaxation processes in the mixture requires a combination of molecular dynamics (MD) simulation, spectroscopy, and analytical considerations.

4. ATR SPECTROSCOPY OF WATER–ETHANOL MIXTURES

Here we are interested in binary mixtures of water and ethanol over the full mixing ratio range from pure water (mole fraction $x_{\mathrm{EtOH}}=0$) to pure ethanol (mole fraction $X_{\mathrm{EtOH}}=1$). The thermodynamic properties of water–ethanol mixtures have been investigated in great detail, partly due to the fact that this specific mixture is very important from a technological and also cultural point of view, and partly because of many intriguing properties of the (at first glance) rather simple system.

We will discuss the measurement of the dielectric function of water–ethanol mixtures. As an extension to our previous studies of water–ethanol mixtures [18,23] we make use of data from a very broad frequency range, by a combination of our own results and already published data recorded in the microwave range with a combination of time-domain reflectometry (TDR) and waveguide interfeometry by Sato and Buchner [24], who has made their original data available to us. By combining the two sets of data we are able to cover the wide frequency range 100 MHz–2.5 THz, and thus we are able to perform accurate fits to the experimental data, covering the full range of dielectric relaxation.

The experimental method used for the recording of our THz data is based on ATR spectroscopy, as described in Section 2 and also described in detail elsewhere [19,20,25]. Briefly, the THz pulse is generated by focussing synchronous, optical pulses from a femtosecond fiber laser (IMRA femtolite, $\lambda=780$ nm, $P_{av}=20$ mW, pulse width of ~90 fs, repetition rate of 50 MHz) onto a biased photoconductive GaAs dipole antenna and detected by use of electro-optic sampling in a ZnTe crystal. A silicon Dove prism is placed at an intermediate focal plane of the THz beam [19]. The principles of generation and detection of pulsed THz radiation as well as the principles of THz-TDS are described, for instance, in [26]. Distilled water (Wako Pure Chemical Industries, Ltd.) and ethanol (Nacalai Tesque, Inc., 99.5% purity) was used without further purification. Water-cooled Peltier elements were used to keep a constant temperature of 25 °C±0.5 °C of the liquid.

The Fresnel reflection coefficients were obtained from the Fourier transformed temporal waveforms with and without a sample, respectively, and these coefficients were used to calculate the complex dielectric function of ethanol–water mixtures at 25 °C for ten different fractions of ethanol, $X_{\mathrm{EtOH}}=0.00$ (H_2O), 0.04, 0.08, 0.11, 0.18, 0.30, 0.50, 0.70, 0.90, and 1.00 (C_2H_5OH).

Figures 3(a) and 3(b) show the real and imaginary part of the complex dielectric function, $\hat{\epsilon}=\epsilon'+i\epsilon''$, of different

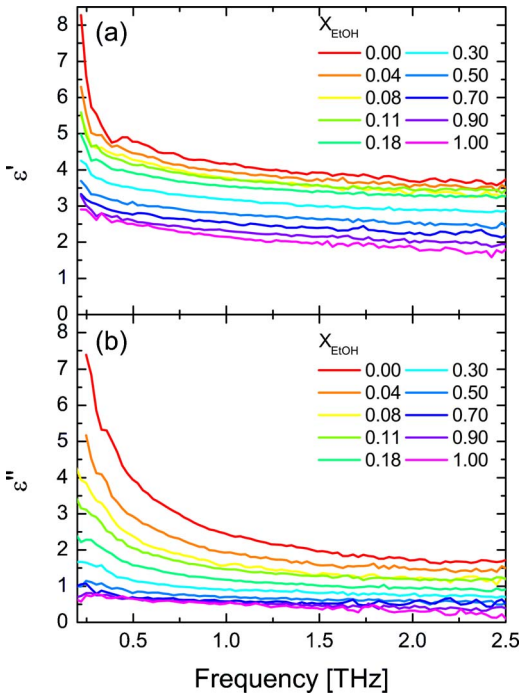

Fig. 3. (Color online) (a) Real and (b) imaginary part of the complex dielectric function of 10 different ethanol–water mixtures at 298 K (25 °C).

mixtures of ethanol (C_2H_5OH) and water (H_2O) as a function of frequency in the region 0.2–2.5 THz.

The measurements presented here are in good agreement with the substantial number of investigations of liquid water in the THz range [12,18,25,27–31], on liquid ethanol [18,28,29], and on mixtures of ethanol and water [18,29].

Since slow relaxation processes in the microwave region contribute substantially to the complex dielectric function, it is necessary to take these into account. Sato and Buchner have previously measured the complex dielectric functions of samples identical to the ones used in this work in the frequency range 0.1–89 GHz using TDR and waveguide interferometry [24]. We have included the measurements of Sato and Buchner in our analysis, and thereby we can cover more than four decades of frequency, from 10^{-4}–2.5 THz. As examples, Fig. 4 shows the complex dielectric function of (a) 18% and (b) 50% ethanol–water mixtures. One can clearly see that, in order to describe all the relaxation processes in ethanol–water mixtures, it is necessary to include data from the microwave region as well as the THz region.

We use a nonlinear fitting procedure based on the Levenberg–Marquardt algorithm to estimate the dielectric parameters by simultaneous fitting to the real and imaginary part of the complex dielectric function, and find that the complex dielectric function of ethanol–water mixtures can be decomposed into three relaxation components and a vibrational term, i.e., we use Eq. (14) with $N=3$ and $M=1$.

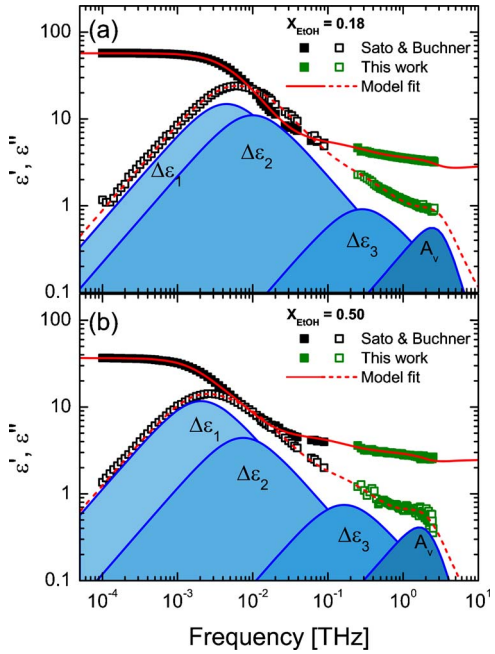

Fig. 4. (Color online) Real (solid symbols) and imaginary (open symbols) part of the complex dielectric function of (a) 11% and (b) 50% ethanol–water mixtures at 298 K (25°). Data recorded in the present work are shown with gray squares (green online), and data from Sato and Buchner [24] are shown in black squares. The fitted dielectric function is shown by solid (real part) and dashed (imaginary part) curves, respectively. The contributions to ϵ'' from the three relaxation processes and the vibrational term are shown in shades of gray (blue online).

Thus our fitting parameters are ϵ_s, $\Delta\epsilon_1$, $\Delta\epsilon_2$, $\Delta\epsilon_3$, and ϵ_∞ and τ_1, τ_2, and τ_3, and finally the vibrational amplitude A_V, angular frequency ω_V, and damping γ_V. It should be pointed out that several of the constants are linked with each other as can be seen by considering the total dielectric strength,

$$\epsilon_s - \epsilon_\infty = \Delta\epsilon_1 + \Delta\epsilon_2 + \Delta\epsilon_3 + \frac{A_V}{\omega_V^2}$$
$$= (\epsilon_s - \epsilon_1) + (\epsilon_1 - \epsilon_2) + \left(\epsilon_2 - \frac{A_V}{\omega_V^2} - \epsilon_\infty\right) + \frac{A_V}{\omega_V^2}, \quad (15)$$

where ϵ_1 and ϵ_2 are the low frequency limits of the intermediate and fast Debye relaxation components, respectively. Liquid water and the 4% mixture are best described by the use of only two Debye terms and one vibration term, i.e., $\Delta\epsilon_2=0$ for these mixtures, and our measurement of liquid ethanol show no sign of an intermolecular stretching vibration, i.e., $A_V=0$ for pure ethanol.

Yada *et al.* recently measured the temperature dependence of the complex dielectric function of water and heavy water with ATR THz spectroscopy [25] up to 3.5 THz and combined their data with microwave data [32,33] and far-infrared data [12]. They found that the complex dielectric function of liquid water at room temperature can be decomposed into four components: a slow relaxation mode at $\tau_1=9.4$ ps, a fast relaxation mode at $\tau_2=0.25$ ps, an intermolecular stretching vibration mode at ~5 THz, and an intermolecular libration mode at ~15 THz. The effect of isotopic substitution on the intermolecular stretch vibration was recently studied, also by Yada *et al.*, where the frequency range of their ATR technique was pushed to 7 THz [34]. Because of the bandwidth limitation (<2.5 THz) in the present work we have not included the intermolecular libration mode in our model.

In Table 1 we compare our fitting results for water with results from the literature. Although variations are seen between the various results, there is a good consistency between the fitted parameters.

In Table 2 our fitting parameters for liquid ethanol are shown together with previous results from Kindt *et al.* [28] and Sato *et al.* [24]. Both groups have used a triple Debye model to describe the relaxation processes of ethanol. Our data is consistent with the work of Kindt *et al.*, while Sato *et al.* report higher values of the high-frequency components (τ_3 and ϵ_∞), which also leads to a shift of the intermediate component (τ_2), most probably due to the lack of high-frequency data in their fitting procedure.

Our fits to the experimental data using Eq. (14) give nearly flat residuals close to zero and a reduced chi-squared $\chi^2 \leq 6\times10^{-3}$ in the entire measurable frequency range for all mixtures.

An overview of the fitted dielectric functions of the different ethanol–water mixtures is presented in Fig. 5. In Figs. 6–11 we summarize all the fitting parameters based on Eq. (14) as function of the ethanol concentration X_{EtOH}.

Table 1. Comparison of Relaxation Parameters of Water

Water	ϵ_s	$\Delta\epsilon_1$	τ_1 [ps]	$\Delta\epsilon_3$	τ_3 [ps]	$A_V/(2\pi)^2$ [THz^2]	$\omega_V/2\pi$ [THz]	$\gamma_V/2\pi$ [THz]	ϵ_∞
This work	78.3	72.3	8.34	2.12	0.36	28.4	5.01	7.06	2.68
Rønne *et al.* [27][a]	80.6[b]	72.1	8.5	1.9	0.17	—	—	—	3.3
Sato *et al.* [24]	78.3	72.2	8.32	2.14	0.39	—	—	—	3.96
Yada *et al.* [25][c]	79.9[b]	74.9	9.43	1.63	0.25	31.5	5.30	5.35	2.50[d]

[a]Measured at 19 °C.

[b]Fixed.

[c]Measured at 20 °C.

[d]Including amplitude of intermolecular libration mode.

In Fig. 6 it is seen that the static dielectric constant ϵ_s decreases with increasing ethanol concentration as observed previously [24,29,35–37]. Also the high-frequency permittivity is seen to decrease monotonically with increasing alcohol concentration.

In Fig. 7 the relaxation amplitudes, normalized to the total contribution to the dielectric constant from the relaxation terms ($\epsilon_s - \epsilon_\infty$) are shown as functions of the ethanol concentration. It is seen that the slow relaxation process is the most prominent, contributing 45–96% to the total dielectric strength. The intermediate and fast process contributes 6.2–48% and 2.4–5.0% to the total dielectric strength, respectively. The slow component shows a minimum near an ethanol concentration of 30% where it contributes to only half of the dielectric strength, whereas for pure water and pure ethanol it contributes to almost all of the dielectric function. The intermediate process shows a similar sequence but with opposite sign and contributes to almost half of the dielectric function in a 30% ethanol–water mixture. This indicates that the slow and intermediate process are strongly correlated. We ensured that the opposite trends seen in the concentration dependencies of $\Delta\epsilon_1$ and $\Delta\epsilon_2$ was not due to simple mathematical interdependence of the variables.

The mixing of ethanol and water at room temperature is an exothermic process where energy is released as the two components are mixed. The amount of released energy per mole of added ethanol, also called the mixing enthalpy ΔH^M, depends on the ethanol concentration [38] and is thus an important indicator of the formation and breaking of intermolecular hydrogen bonds during the mixing process. Interestingly, there seems to be a strong correlation between $\Delta\epsilon_1$, $\Delta\epsilon_2$, and ΔH^M of the solution. This correlation is detailed in Fig. 8, which shows the concentration dependence of the mixing enthalpy ΔH^M for ethanol–water mixtures (red curve [39]) together with the relative strengths of the slow (black squares) and intermediate (blue circles) relaxation processes.

In Fig. 9 we show the concentration dependence of the three relaxation times in the model. Figure 9(a) shows that the slow relaxation time, τ_1, has a nearly linear dependence of the ethanol concentration, in agreement with previous studies. In general, previous studies in the low-frequency region firmly characterizes the slow relaxation process [24,35–37] due to the facts that (a) this process occurs within their spectral range and (b) that the slow relaxation process is the most dominant of all the relaxation processes.

Figures 9(b) and 9(c) show the concentration dependence of the intermediate (τ_2) and fast (τ_3) relaxation processes. In contrast to the behavior of τ_1, τ_2 (and to some extent also τ_3) displays a nonmonotonous behavior with ethanol concentration, with a maximum of τ_2 at $X_{\mathrm{EtOH}} \approx 0.3-0.4$.

Similar to the concentration dependence of the mixing enthalpy, the mixing volume (volume change per added ethanol) of ethanol–water mixtures display a nonmonotonous behavior. In Fig. 10 we plot the normalized mixing volume $\Delta V_{mix}/n_T$ (solid, red curve), where n_T is the total number of molecules in the mixture, as function of X_{EtOH}. In the same graph we show the normalized values of τ_2 (black squares). It is apparent that there is a strong correlation between the mixing volume and the time constants of the intermediate and fast relaxation processes.

The reduction of the volume during the mixing process indicates a closer packing of the molecules in the liquid. Although detailed numerical simulation of this process is required, we speculate that the correlation between $\Delta V_{mix}/n_T$ and τ_2 is consistent with a slowing down of the relaxation processes due to less space available for the re-

Table 2. Comparison of Relaxation Parameters of Ethanol

Ethanol	ϵ_s	$\Delta\epsilon_1$	τ_1 [ps]	$\Delta\epsilon_2$	τ_2 [ps]	$\Delta\epsilon_3$	τ_3 [ps]	ϵ_∞
This work	24.4	20.0	163	1.40	4.51	1.21	0.33	1.85
Kindt *et al.* [28][a]	24.4[b]	20.2	161	1.43	3.3	0.79	0.22	1.93
Sato *et al.* [24]	24.5	20.0	165	0.74	10.4	1.19	1.69	2.60

[a]Measured at room temperature.

[b]Fixed.

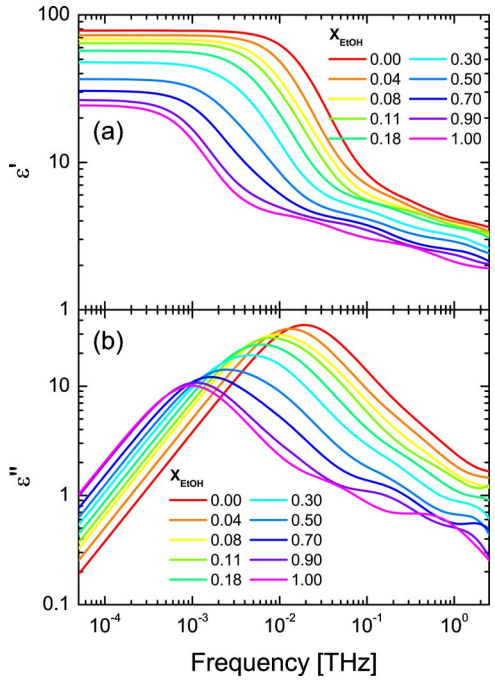

Fig. 5. (Color online) Fitted curves of (a) the real and (b) the imaginary part of the complex dielectric functions for different ethanol–water mixtures by using Eq. (14).

laxation processes. This would then indicate that the intermediate relaxation processes are of intermolecular nature.

This interpretation is further supported by MD simulations [40] and experimental data [41], which show that the mutual diffusion coefficients for ethanol–water mixtures are smallest in the region near $X_{\mathrm{EtOH}}=0.3$, and the self-diffusion coefficients of water in ethanol–water mixtures is smallest in the region near $X_{\mathrm{EtOH}}=0.4$.

The parameters for the intermolecular stretching vibration mode are plotted in Fig. 11. As previously mentioned, the vibration parameters of water are consistent with the findings of Yada *et al.*

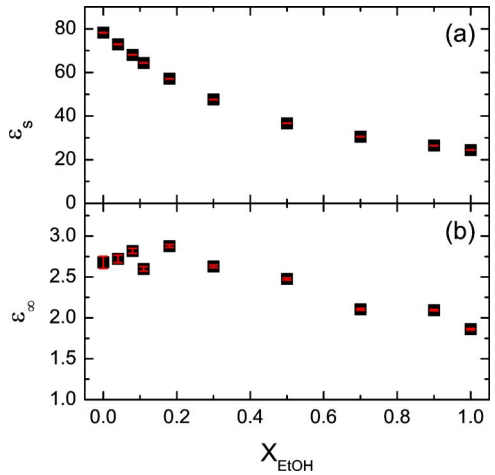

Fig. 6. (Color online) Fitted values and standard deviations of (a) the static dielectric constant, ϵ_s, and (b) the dielectric constant in the high frequency limit, ϵ_∞, of ethanol–water mixtures as a function of ethanol fraction X_{EtOH}.

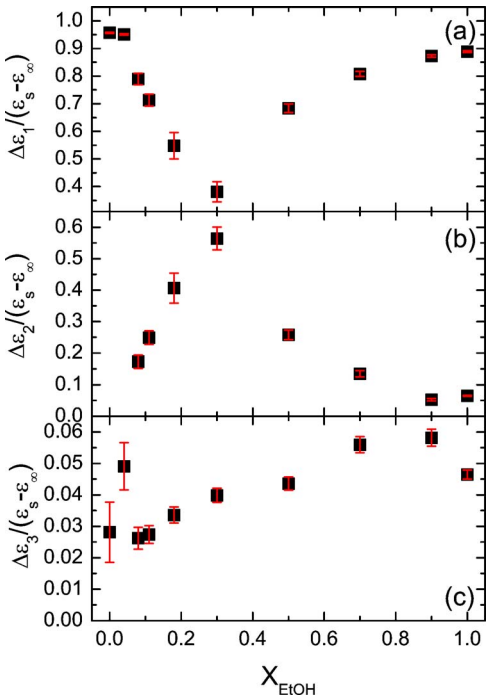

Fig. 7. (Color online) Debye relaxation strengths (a) $\Delta\epsilon_1$, (b) $\Delta\epsilon_2$, and $\Delta\epsilon_3$, normalized to the full dielectric strength $\epsilon_s-\epsilon_\infty$, of ethanol–water mixtures as functions of the ethanol concentration.

Since intermolecular vibrations occur in pure water, they are also bound to be present in ethanol–water mixtures to some extent. In the water-rich region the vibrational mode shifts to lower frequencies as the ethanol concentration increases, and it levels out above 30% to a frequency around 2.5 THz. One possible explanation of the frequency decrease could be that when ethanol is added to water some of the water molecules participating in the intermolecular vibrational motion will be substituted with heavier ethanol molecules resulting with an overall frequency drop. At this stage it is not clear why the resonance frequency remains fixed at higher ethanol concentrations. However, it is interesting to note that the resonance frequency remains fixed for concentrations above that of the minimum in the mixing enthalpy and

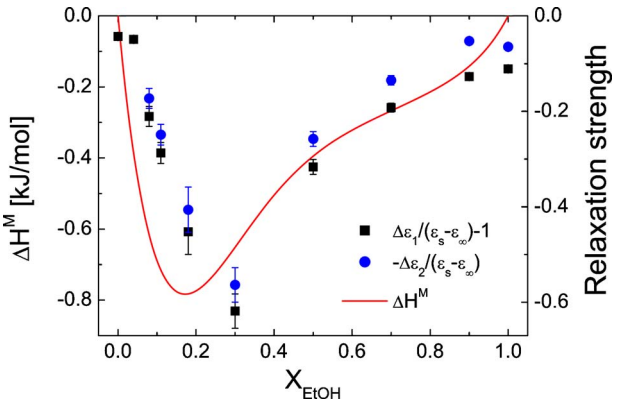

Fig. 8. (Color online) Mixing enthalpy of ethanol/water mixtures (red curve, from [39]) and the relaxation strengths of the slow Debye process (black points) as a function of ethanol concentration

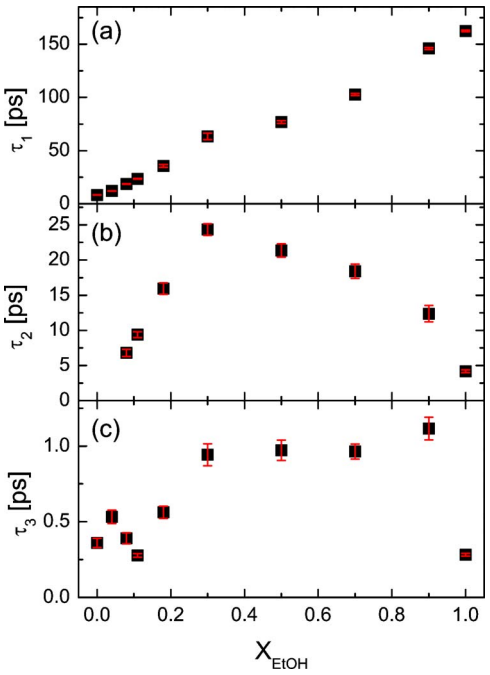

Fig. 9. (Color online) Debye relaxation times (a) τ_1, (b) τ_2, and (c) τ_3 of ethanol–water mixtures as a function of ethanol concentration.

approximately where the self-diffusion and mutual diffusion coefficients display their minima, as discussed above.

For pure ethanol our data indicate that the vibrational mode no longer contributes significantly to the dielectric function, indicating that water must be present in order to observe the effects of the mode.

5. INSPECTION OF LIQUIDS INSIDE BOTTLES

A wide range of glasses and polymers are transmissive to THz radiation. At the same time, typical surface quality of bottles for commercial liquids is sufficient for undisturbed transmission of THz radiation due to its long wavelength. Hence inspection of liquids inside bottles and other containers with THz radiation is possible. It has previously been demonstrated that it is possible to determine the alcohol content of a water–ethanol mixture inside polythylene teraphthalate (PET) and glass bottles [23]. In Fig. 12 the experimental configuration of the measurement on a bottle is shown. In this configuration the bottle wall itself is used as the interface to the liquid, thus lifting the requirement of removing the liquid from the bottle before the measurement.

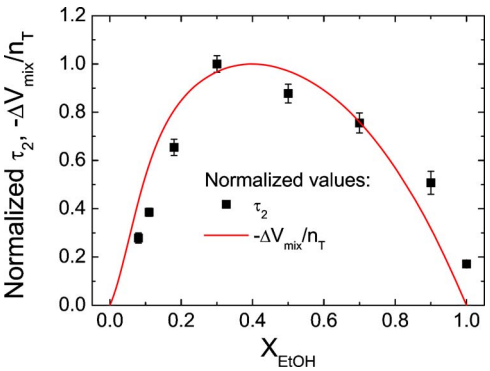

Fig. 10. (Color online) Mixing volume of ethanol–water mixtures (solid, red curve) and the time constants τ_2 (black squares).

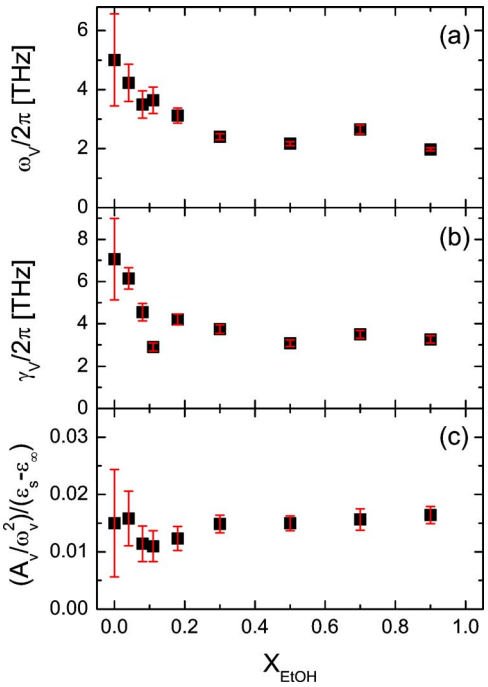

Fig. 11. (Color online) (a) Resonance frequency, (b) damping constant, and (c) vibration strength of the intermolecular stretching vibration of ethanol–water mixtures as a function of ethanol concentration.

The PET bottle wall has an index of refraction of approximately 1.75 in the 0.2–1.5 THz range [23]. While this index is significantly lower than that of water in the same range, the PET index is similar to that of certain other polar liquids, such as dioxan. In Fig. 13 we show the reflected THz signal from a PET bottle containing either water, ethanol, or dioxan. Each trace consists of two reflected portions of the same input signal, namely, the reflection from the outer surface of the bottle and, slightly delayed due to propagation through the bottle material, a second reflection from the interface between the bottle wall and the liquid.

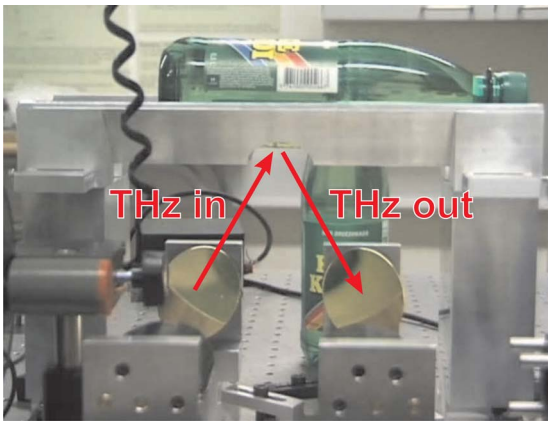

Fig. 12. (Color online) Self-referenced THz reflection spectroscopy of liquid inside a PET bottle.

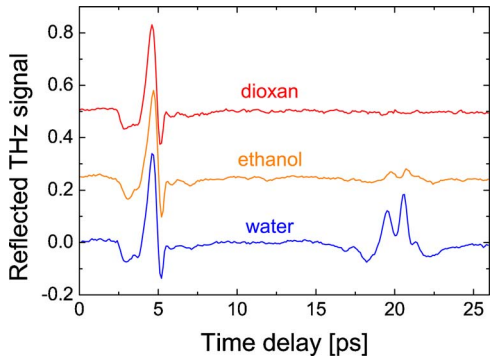

Fig. 13. (Color online) Reflected THz traces from a PET bottle containing water (lower trace), ethanol (middle trace), and dioxan (upper trace).

The reflected signal from the water-filled bottle shows a clear reflection from the PET–water interface. The corresponding reflection from the PET–ethanol interface in the ethanol-filled bottle shows a much weaker reflection amplitude due to the lower index of refraction of the liquid ethanol. When the bottle is filled with dioxan the second reflection virtually disappears, indicating very good index matching between PET and dioxan. Our observation of good index matching between PET ($n \approx 1.75$) and dioxan is not in complete agreement with previous determination of the index of refraction of pure dioxan [42] where the index of refraction was ported to decrease monotonically from 1.48–1.46 in the 0.5–2.5 THz range. We believe that this minor discrepancy is insignificant, and possibly due to impurities (such as water traces) in the dioxan used in our experiment, where no special precautions were taken to avoid water contamination.

The disappearance of the signal from the interface between the bottle wall and the liquid of course hinders any detailed analysis of the bottle content. However, the lack of a second reflection actually indicate that the PET bottle is filled with a liquid of relatively low refractive index, which on its own is useful information in some situations. Many volatile liquids, which at the same time are highly flammable, will have a low index of refraction, and thus THz reflection spectroscopy may be used for detection of flammable liquids in PET containers.

6. DIELECTRIC RELAXATION IN HYDROGEN PEROXIDE AND FUELS

Another class of hazardous liquids are oxidizers, which in connection with fuel components may form explosive mixtures. Thus there is a high demand for methods for standoff detection of liquids that may be used for the fabrication of liquid explosives. In this section we discuss reflection THz-TDS measurements of the dielectric properties of the oxidizer hydrogen peroxide as well as the fuel components nitromethane and nitroethane.

In Fig. 14(a) we show THz reflection traces from a PET bottle with a wall thickness of 0.65 mm, filled with water (blue trace) and a standard 30% (by weight) solution of hydrogen peroxide (red trace), a strong oxidizing and bleaching agent.

The reflected signal from the two liquids are virtually indistinguishable, immediately indicating that the dielectric properties of the hydrogen peroxide solution are very similar to those of pure water. This is further demonstrated in Fig. 14(b), where the real and imaginary part of the dielectric function of pure water (blue traces) are compared to those of the hydrogen peroxide solution (red traces). Within the signal-to-noise ratio of the experiment the two dielectric functions are identical. Previous reports showed little variation of the static dielectric constant of hydrogen peroxide solutions at room temperature [43–45], in agreement with the results published here.

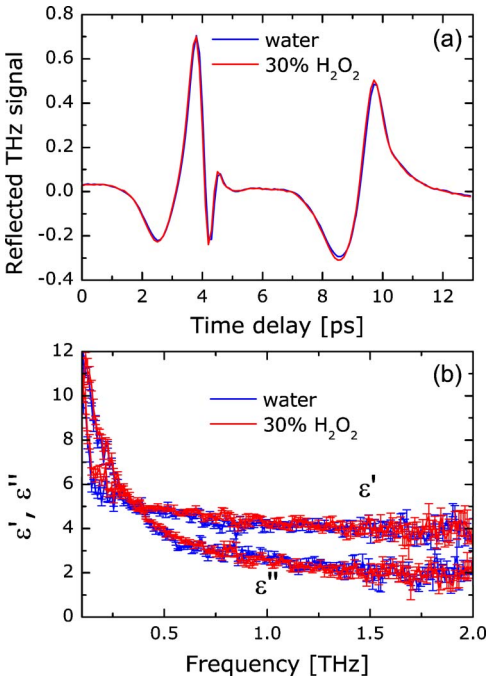

Fig. 14. (Color online) (a) Reflected THz traces from a PET surface in contact with water (blue trace) and a 30% hydrogen peroxide solution (red trace). (b) Real and imaginary part of the dielectric function of water (blue traces) and a 30% hydrogen peroxide solution (red traces). The error bars indicate the standard deviation between five consecutive scans.

One of the reasons for the striking similarity between liquid water and an aqueous solution of hydrogen peroxide is that the hydrogen peroxide molecule is isomorphous with the water molecule, i.e., it has a tetragonal electronic structure [45], and thus it can be incorporated into the intermolecular water structure with the same coordination number. Thus the intermolecular hydrogen bond network is left rather undisturbed by the addition of hydrogen peroxide, compared to the effect of solvating other molecules in water. At this point we dare to speculate that spectroscopy with higher spectral bandwidth may help to shed further light on the apparent similarity between liquid water and concentrated solutions of hydrogen peroxide.

Interestingly, the dielectric properties in the THz range of some non-hydrogen-bonded liquids are also well described by Debye-type relaxation processes, and thus in some aspects the dielectric properties of such liquids can be quite similar to those of liquid water. Here we consider the liquid fuels nitromethane (NM, molecular formula CH_3NO_2) and nitroethane (NE, molecular formula $CH_3CH_2NO_2$). The dominating attractive intermolecular forces in NM are dipole–dipole interactions [46], with

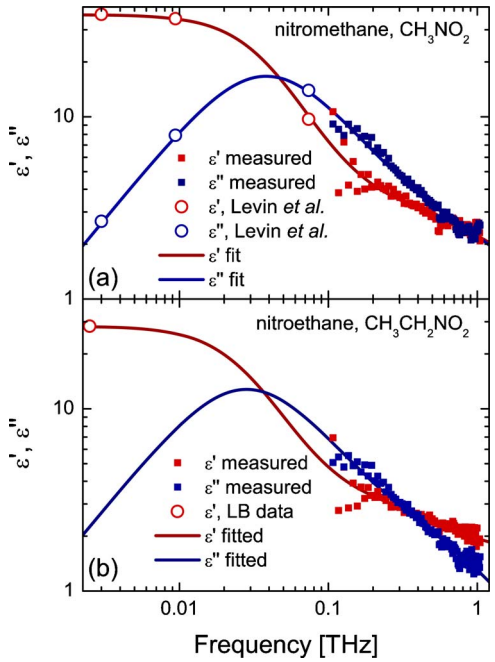

Fig. 15. (Color online) Complex permittivity of (a) nitromethane and and (b) nitroethane. Solid gray (red online) symbols and solid black (blue online) symbols represent our THz measurements, open symbols are literature values [48,49], solid lines are fits using the double Debye model to the available experimental data.

little or no intermolecular hydrogen bonding [47]. We assume similar intermolecular interactions in liquid NE, although very little information about the intermolecular interactions in liquid NE is available in the literature.

In Fig. 15(a) we show the complex dielectric function of NM, and in Fig. 15(b) the dielectric function of NE. The solid symbols represent our measurements in the 0.1–1.2 THz frequency range, and the open symbols are literature values. We use the few low-frequency values of the complex permittivity that are reported for NM [48], as well as the static permittivity of NE [49]. The combined experimental data are well fitted by a double Debye model, including two relaxation processes. The fitted curves of the real and imaginary parts of the permittivity of NM and NE are shown as solid lines in Figs. 15(a) and 15(b).

The best fitting parameters and their standard errors are given in Table 3. The characteristic relaxation times of 4.18 and 5.67 ps for NM and NE, respectively, are shorter than the slowest relaxation time of water (8.3 ps). This is consistent with a picture where the slowest relaxation process is related to intermolecular motion of the whole molecules. The weaker intermolecular bonds in NM and NE could then lead to a somewhat faster relaxation than is observed in bulk water. Further, the slightly slower relaxation process in NE than in NM is consistent with the larger dimensions of the NE molecules with respect to the NM molecules.

The slow relaxation process is much stronger than the faster relaxation process in both NM and NE, by the same ratio $\Delta\epsilon_1/\Delta\epsilon_2 \approx 18$, possibly again hinting at similar intermolecular dynamics in the two liquids. The corresponding ratio in liquid water is twice as large, indicating that the fast relaxation processes in NM and NE are more prominent than in water.

7. SUMMARY AND CONCLUSIONS

Water remains a liquid with many intriguing properties. The physical and optical properties of water and other polar liquids in the THz frequency range has been studied both by precise molecular dynamics simulations and by optical spectroscopy, with simulation results indicating that there is a connection between the microscopic dynamics and structure of the liquid and its thermodynamic properties. The link between optical experiments and the dynamics of the liquid is often to apply a phenomenological relaxation model to the dielectric spectrum of the liquid, and thus obtain information about the strength of the relaxation processes and their characteristic time constants. The most prominent modeling tool for this purpose is the Debye model, often with the inclusion of several relaxation processes which are then assumed to take place in a parallel fashion. This approach has given the possibility of identifying several relaxation processes in water and ethanol–water mixtures.

Broadband spectroscopy that includes information about the lowest-frequency intermolecular vibrational modes of the liquid has made it possible to combine data from DC measurements, the microwave regime, and the low and high THz regime, to obtain complete coverage of the frequency range that contains all the relaxation processes.

In our paper we have used such an approach to combine already published microwave data with our measurements of the dielectric function of water, ethanol–water mixtures, ethanol, aqueous solutions of hydrogen peroxide, and the fuels nitromethane and nitroethane. All these liquids were found to be well described by the Debye relaxation model with two (water, hydrogen peroxide solution, nitromethane, nitroethane) or three (water–ethanol mixtures and ethanol) relaxation terms. In the case of water and water–ethanol mixtures, the presence of the lowest intermolecular vibrational mode influences our data, and this mode was included in the modeling.

We found that the characteristics of the relaxation processes (relaxation strength and relaxation time constants) are correlated with the macroscopic thermodynamic prop-

Table 3. Relaxation Parameters for Nitromethane and Nitroethane

	ϵ_s	$\Delta\epsilon_1$	$\Delta\epsilon_2$	ϵ_∞	τ_1 [ps]	τ_2 [ps]
Nitromethane	36.4±0.7	33.3±0.7	1.89±0.20	1.26±0.17	4.18±0.12	0.16±0.02
Nitroethane	28.4[a]	25.4±0.1	1.39±0.12	1.60±0.06	5.67±0.14	0.29±0.03

[a]Kept fixed during fitting, value from [49]

erties of the liquid. Specifically it seems like there is a strong correlation between the mixing volume of ethanol–water mixtures and the intermediate and fast relaxation times—the smaller the mixing volume, the slower these relaxation times appear to be. Similarly, the largest enthalpy of mixing of ethanol–water mixtures appear at an ethanol concentration where the strength of the slow relaxation process is smallest and the strength of the intermediate relaxation process is highest.

We also found that the slow and intermediate relaxation times in the dipole–dipole correlated fuels nitromethane and nitroethane are approximately twice as fast as the corresponding times in water. Furthermore, the relative strength of the intermediate process with respect to the slow process is twice as large as the corresponding ratio in water. This we interpret as an indication of the smaller intermolecular forces in liquid nitromethane and nitroethane compared to the hydrogen-bonded water.

We suggest that THz-TDS measurements may be a useful tool for the distinction between benign liquids such as water and less concentrated ethanol–water solutions and hazardous liquids such as fuels and organic solvents. Some hazardous liquids, such as hydrogen peroxide, seem indistinguishable from pure water by their THz dielectric properties. However, increased spectral coverage to higher frequencies may shed further light on any differences in the relaxation dynamics of hydrogen peroxide and water.

The frequency coverage of the THz-TDS system is an important factor for the interpretation of the results. Based on the results presented here it is obvious that it is not possible to rely solely on data in the low THz region, since the faster processes are not covered by such experiments. We therefore believe that the ongoing progress on the improvement of bandwidth of THz-TDS systems, for instance by ultrabroadband photoconductive emitters and detectors or novel nonlinear crystals for ultrabroadband THz generation, and detection by electrooptic processes, will be very important for the progress of the experimental verification of numerical results. Furthermore, the low-frequency range, up to 0.1 THz, which is well-covered by microwave dielectric spectroscopy, plays a major role. Thus, spectroscopic studies that include both microwave techniques and the broadband THz techniques are important in order to obtain a complete picture of the extremely broadband relaxation processes in polar liquids.

ACKNOWLEDGMENTS

We thank Richard Buchner and Takaaki Sato for making their original spectroscopic data on water-ethanol mixtures available to us. We acknowledge the EU project TeraNova and the H. C. Ørsted Foundation for partial financial support. One of the authors (K.T.) acknowledges support from The Ministry of Education, Culture, Sports, Science and Technology (MEXT) of Japan (Grant-in-Aid for Creative Scientific Research program, 18GS0208).

REFERENCES

1. D. J. Segelstein, "The complex refractive index of water," M.S. thesis (Univ. of Missouri-Kansas City, 1981). Data can be found at http://www.philiplaven.com/p20.html.
2. T. Arikawa, M. Nagai, and K. Tanaka, "Characterizing hydration state in solution using terahertz time-domain attenuated total reflection spectroscopy," Chem. Phys. Lett. **457**, 12–17 (2008).
3. U. Heugen, G. Schwaab, E. Bründermann, M. Heyden, X. Yu, D. M. Leitner, and M. Havenith, "Solute-induced retardation of water dynamics probed directly by terahertz spectroscopy," Proc. Natl. Acad. Sci. U.S.A. **103**, 12301–12306 (2006).
4. M. Heyden, E. Bründermann, U. Heugen, G. Niehues, D. M. Leitner, and M. Havenith, "Long-range influence of carbohydrates on the solvation dynamics of water—Answers from terahertz absorption measurements and molecular modeling simulations," J. Am. Chem. Soc. **130**, 5773–5779 (2008).
5. D. M. Mittleman, M. C. Nuss, and V. L. Colvin, "Terahertz spectroscopy of water in inverse micelles," Chem. Phys. Lett. **275**, 332–338 (1997).
6. J. E. Boyd, A. Briskman, V. L. Colvin, and D. M. Mittleman, "Direct observation of terahertz surface modes in nanometer-sized liquid water pools," Phys. Rev. Lett. **87**, 147401 (2001).
7. J. E. Boyd, A. Briskman, C. M. Sayes, D. Mittleman, and V. Colvin, "Terahertz vibrational modes of inverse micelles," J. Phys. Chem. B **106**, 6346–6353 (2002).
8. J. Zhang and D. Grischkowsky, "Waveguide terahertz time-domain spectroscopy of nanometer water layers," Opt. Lett. **29**, 1617–1619 (2004).
9. J. Zhang and D. Grischkowsky, "Terahertz time-domain spectroscopy of submonolayer water adsorption in hydrophilic silica aerogel," Opt. Lett. **29**, 1031–1033 (2004).
10. P. Uhd Jepsen and B. M. Fischer, "Dynamic range in terahertz time-domain transmission and reflection spectroscopy," Opt. Lett. **30**, 29–31 (2005).
11. T. J. Parker, "Dispersive Fourier transform spectroscopy," Contemp. Phys. **31**, 335–353 (1990).
12. M. N. Afsar and J. B. Hasted, "Measurements of the optical constants of liquid H_2O and D_2O between 6 and 450 cm^{-1}," J. Opt. Soc. Am. **67**, 902–904 (1977).
13. D. Grischkowsky, S. Keiding, M. van Exter, and Ch. Fattinger, "Far-infrared time-domain spectroscopy with terahertz beams of dielectrics and semiconductors," J. Opt. Soc. Am. B **7**, 2006–2015 (1990).
14. M. van Exter, Ch. Fattinger, and D. Grischkowsky, "Terahertz time-domain spectroscopy of water vapor," Opt. Lett. **14**, 1128–1130 (1989).
15. P. Uhd Jepsen, R. H. Jacobsen, and S. R. Keiding, "Generation and detection of terahertz pulses from biased semiconductor antennas," J. Opt. Soc. Am. B **13**, 2424–2436 (1996).
16. A. Nahata, A. S. Weling, and T. F. Heinz, "A wideband coherent terahertz spectroscopy system using optical rectification and electro-optic sampling," Appl. Phys. Lett. **69**, 2321–2323 (1996).
17. L. Thrane, R. H. Jacobsen, P. Uhd Jepsen, and S. R. Keiding, "THz reflection spectroscopy of liquid water," Chem. Phys. Lett. **240**, 330–333 (1995).
18. P. Uhd Jepsen, U. Møller, and H. Merbold, "Investigation of aqueous alcohol and sugar solutions with reflection terahertz time-domain spectroscopy," Opt. Express **15**, 717–737 (2007).
19. M. Nagai, H. Yada, T. Arikawa, and K. Tanaka, "Terahertz time-domain attenuated total reflection spectroscopy in water and biological solution," Int. J. Infrared Millim. Waves **27**, 505–515 (2006).
20. H. Hirori, M. Nagai, and K. Tanaka, "Destructive interference effect on surface plasmon resonance in terahertz attenuated total reflection," Opt. Express **13**, 10801–10814 (2005).
21. N. E. Hill, W. E. Vaughan, A. H. Price, and M. Davis,

Dielectric Properties and Molecular Behaviour (Van Nostrand Reinhold Company, 1969).
22. R. M. Hill and L. A. Dissado, "Debye and non-Debye relaxation," J. Phys. C **18**, 3829–3836 (1985).
23. P. Uhd Jepsen, J. K. Nielsen, and U. Møller, "Characterization of aqueous alcohol solutions in bottles with THz reflection spectroscopy," Opt. Express **16**, 9318–9331 (2008).
24. T. Sato and R. Buchner, "Dielectric relaxation processes in ethanol/water mixtures," J. Phys. Chem. A **108**, 5007–5015 (2004).
25. H. Yada, M. Nagai, and K. Tanaka, "Origin of the fast relaxation component of water and heavy water revealed by terahertz time-domain attenuated total reflection spectroscopy," Chem. Phys. Lett. **464**, 166–170 (2008).
26. *Terahertz Spectroscopy: Principles and Applications* S. Dexheimer, ed. (CRC Press, 2007).
27. C. Rønne, L. Thrane, P.-O. Astrand, A. Wallqvist, K. V. Mikkelsen, and S. R. Keiding, "Investigation of the temperature dependence of dielectric relaxation in liquid water by THz reflection spectroscopy and molecular dynamics simulation," J. Chem. Phys. **107**, 5319–5331 (1997).
28. J. T. Kindt and C. A. Schmuttenmaer, "Far-Infrared dielectric properties of polar liquids probed by femtosecond terahertz pulse spectroscopy," J. Phys. Chem. **100**, 373–379 (1996).
29. H. Kitahara, T. Yagi, K. Mano, M. W. Takeda, S. Kojima, and S. Nishizawa, "Dielectric characteristics of water solutions of ethanol in the terahertz region," J. Korean Phys. Soc. **46**, 82–85 (2005).
30. J. B. Hasted, S. K. Husain, F. A. M. Frescura, and J. R. Birch, "The temperature variation of the near millimetre wavelength optical constants of water," Infrared Phys. **27**, 11–15 (1987).
31. J. Barthel, K. Bachhuber, R. Buchner, and H. Hetzenauer, "Dielectric spectra of some common solvents in the microwave region. Water and lower alcohols," Chem. Phys. Lett. **165**, 369–373 (1990).
32. U. Kaatze, "Complex permittivity of water as a function of frequency and temperature," J. Chem. Eng. Data **34**, 371–374 (1989).
33. J. M. Alison and R. J. Sheppard, "A precision waveguide system for the measurement of complex permittivity of lossy liquids and solid tissues in the frequency range 29 GHz to 90 GHz—III. The liquid system for 57 to 82 GHz: an investigation into water and formamide," Meas. Sci. Technol. **2**, 975–979 (1991).
34. H. Yada, M. Nagai, and K. Tanaka, "The intermolecular stretching vibration mode in water isotopes investigated with broadband terahertz time-domain spectroscopy," Chem. Phys. Lett. **473**, 279–283 (2009).
35. S. Mashimo, S. Kuwabara, S. Yagihara, and K. Higasi, "The dielectric relaxation of mixtures of water and primary alcohol," J. Chem. Phys. **90**, 3292–3294 (1989).
36. T. Sato, A. Chiba, and R. Nozaki, "Dynamical aspects of mixing schemes in ethanol-water mixtures in terms of the excess partial molar activation free energy, enthalpy, and entropy of the dielectric relaxation process," J. Chem. Phys. **110**, 2508–2521 (1999).
37. P. Petong, R. Pottel, and U. Kaatze, "Water-ethanol mixtures at different compositions and temperatures. A dieletric relaxation study," J. Phys. Chem. A **104**, 7420–7428 (2000).
38. R. Chang, *Physical Chemistry for the Chemical and Biological Sciences*, 3rd ed. (University Science Books, 2000).
39. J. A. Boyne and A. G. Williamson, "Enthalpies of mixture of ethanol and water at 25 °C," J. Chem. Eng. Data **12**, 318 (1967).
40. C. Zhang and X. Yang, "Molecular dynamics simulation of ethanol/water mixtures for structure and diffusion properties," Fluid Phase Equilib. **231**, 1–10 (2005).
41. M. T. Tyn and W. F. Calus, "Temperature and concentration dependence of mutual diffusion coefficients of some binary liquid systems," J. Chem. Eng. Data **20**, 310–316 (1975).
42. S. Schrödle, B. Fischer, H. Helm, and R. Buchner, "Picosecond dynamics and microheterogenity of water +dioxane mixtures," J. Phys. Chem. A **111**, 2043–2046 (2007).
43. P. M. Gross, Jr. and R. C. Taylor, "The dielectric constants of water, hydrogen peroxide, and hydrogen peroxide-water mixtures," J. Am. Chem. Soc. **72**, 2075–2080 (1950).
44. A. K. Lyaschenko, V. S. Goncharov, and P. S. Yastremskii, "Structure and dielectric properties of aqueous solutions of hydrogen peroxide," J. Struct. Chem. **17**, 871–876 (1976).
45. A. A. Potapov and I. Yu. Parkhomenko, "Dielectric properties of solutions isomorphous with water," Russian J. Gen. Chem. **75**, 34–39 (2005).
46. D. C. Sorescu, B. M. Rice, and D. L. Thompson, "Molecular dynamics simulations of liquid nitromethane," J. Phys. Chem. A **105**, 9336–9346 (2001).
47. H. E. Alper, F. Abu-Awwad, and P. Politzer, "Molecular dynamics simulations of liquid nitromethane," J. Phys. Chem. B **103**, 9738–9742 (1999).
48. V. V. Levin, E. A. Ovsoyan, and V. I. Ovchinnikov, "Dispersion of the dielectric constant of nitromethane," Russian J. Phys. Chem. **45**, 1333–1334 (1971).
49. O. Madelung, ed. *Numerical Data and Functional Relationships in Science and Technology*, Vol. 6 of Static Dielectric Constants of Pure Liquids and Binary Liquid Mixtures (Springer, 1991).